# Inverse stability problem in beam dynamics

Alexey Burov*
*Fermilab, PO Box 500, Batavia, Illinois 60510-5011, USA*

(Received 22 July 2022; revised 29 June 2023; accepted 3 August 2023; published 17 August 2023)

Beam stability is conventionally described by means of the stability diagram, which is a threshold line in a complex plane of a particular intensity parameter, the coherent tune shift; the diagram separates stable and unstable states. The incoherent tune spread of the beam particles normally causes the transverse stability diagram to be an asymmetric bell-shaped curve above the real axis; for a given optical nonlinearity, the diagram is determined by the beam distribution function only. Recently, such a diagram was measured by means of an antidamper, see Antipov *et al.*, Phys. Rev. Lett. **126**, 164801 (2021). Such measurements open the door to a new method of beam diagnostics, finding the beam phase space density as a solution of an *inverse stability problem*. The main idea, methods of its implementation, possible obstacles and optimizations are discussed.

DOI: 10.1103/PhysRevAccelBeams.26.082801

## I. INTRODUCTION

For a start, let us consider a bunch of $N$ particles with slightly different oscillation frequencies, so that their spread $\bar{\Delta}\omega$ is small compared to the average value $\bar{\omega}$. Let us assume also that besides the slightly nonlinear focusing, there is a feedback which detects the centroid offset and acts on the bunch as a whole proportionally to that. For such a system, it is convenient to introduce slow amplitudes of the particle oscillations, $a_k = \exp(i\bar{\omega}t)x_k$, where $x_k$ is the offset of the $k$th particle, and $t$ is time. Due to the nonlinearity and the feedback, the amplitudes are not constant, but obey the dynamic equations,

$$\dot{a}_k + i\Delta\omega_k a_k = -ig\bar{a}, \tag{1}$$

where $\bar{a} = \sum_k a_k/N$ is the slow amplitude of the bunch centroid, $\Delta\omega_k$ is the tune shift of the $k$th particle, and $g$ is the feedback gain in units of the tune shift. Looking for the solution $a_k \propto \exp(-i\nu t)$, one gets

$$a_k = \frac{g}{\nu - \Delta\omega_k}\bar{a}. \tag{2}$$

Averaging that over the particles leads to the dispersion equation for the eigenfrequency $\nu$,

$$\frac{g}{N}\sum_k \frac{1}{\nu - \Delta\omega_k} = 1. \tag{3}$$

If the frequency spread $\Delta\omega$ is caused by nonlinearity of transverse focusing of the particles with incoherent transverse actions $J_x$, $J_y$, then $\Delta\omega_k = \Delta\omega(J_x, J_y)$, and the dispersion equation can be presented by means of the integral with the bunch distribution function $F(J_x, J_y)$,

$$-\left[\int\int \mathrm{d}J_x \mathrm{d}J_y \frac{J_x \frac{\partial F}{\partial J_x}}{\nu - \Delta\omega(J_x, J_y) + io}\right]^{-1} = g. \tag{4}$$

Here we followed the Hereward rule [1] for the sum to integral transformation,

$$\frac{1}{N}\sum_k (\ldots) \to -\int\int \mathrm{d}J_x \mathrm{d}J_y J_x \frac{\partial F}{\partial J_x}(\ldots) \tag{5}$$

and applied the Landau rule for the pole, $\nu \to \nu + io$, with an infinitesimally small $o > 0$; all integrals over the actions are from zero to infinity. The distribution function is supposed to be normalized, $\int\int \mathrm{d}J_x \mathrm{d}J_y F(J_x, J_y) = 1$. The asymmetry between $x$ and $y$ in Eq. (5) is caused by $x$-direction of the oscillations.

Instead of solving the dispersion equation (4) for the eigenvalue $\nu$ for a given complex gain $g$, the problem can be reversed: on the complex plane of the gain $g$, let us find the line which separates stable and unstable states of the bunch. For this purpose, the dispersion equation can be considered as a map $\nu \to g$, so this threshold line is generated by mapping of the real axis of $\nu$ onto the complex plane of $g$ by means of Eq. (4). Threshold lines of such a kind are called *stability diagrams*. For beam dynamics, they were

*burov@fnal.gov

introduced by Vaccaro [2,3], so there is a reason to call them *Vaccaro diagrams*.

The considered case of the bunch-flat feedback, or the *antidamper*, allows a generalization for an arbitrary wake function. In fact, the same dispersion equation (4) is valid for any wake function; instead of the gain $g$ the *coherent tune shift* $\Omega$ has to be used, which is the tune shift of the collective mode in case of no tune spread. Thus, for an arbitrary wake,

$$-\left[\int\int \mathrm{d}J_x \mathrm{d}J_y \frac{J_x \frac{\partial F}{\partial J_x}}{\nu - \Delta\omega(J_x, J_y) + io}\right]^{-1} = \Omega; \quad (6)$$

see more details in Refs. [4,5].

Without wakes but with the antidamper, the bunch is stable provided that the gain $g$ lies below the Vaccaro diagram. Otherwise, the rigid-bunch collective mode, or zeroth mode, would be unstable. For the wake-driven instabilities, the bunch is stable if and only if each of its collective tune shifts lies below the Vaccaro diagram.

The possibility for the bunch to be stable even if the feedback or the wake are destabilizing to some degree is a demonstration of the *Landau damping*, a self-stabilizing mechanism based on the resonance interaction between the coherent and incoherent degrees of freedom, i.e., the resonance between collective modes and individual particles [6,7].

Historically, the idea of the stability diagram has been suggested and then used for decades for the case of wakes and machine impedances, not for the antidampers. The latter was proposed as a way to measure the diagram, making use of our ability to change the complex gain, while the machine wake function is normally just given. The proposed idea was recently implemented at the LHC by Antipov *et al.* [8].

Measuring of the stability diagram opens the door to a specific beam diagnostics. Indeed, with known incoherent tune dependence $\Delta\omega(J_x, J_y)$, the Vaccaro diagram is determined by the distribution function only. Obviously, the entire distribution function $F(J_x, J_y)$ cannot be obtained from such measurements: a function of two arguments is not extractable from a function of one argument, which Vaccaro diagram is. We will see below, that what can be generally extracted from a single diagram, are two 1D projections of the full distribution, $F_x(J_x) = \int \mathrm{d}J_y F(J_x, J_y)$ and $F_y(J_y) = \int \mathrm{d}J_x F(J_x, J_y)$. Such an objective can be called the *diagram inversion problem*. Indeed, the conventional forward problem requires finding the diagram when the distribution function is given. The inverse problem requires the opposite: finding the distribution function when the diagram is given. Such inversion of the diagram can be treated as a particular case of the *inverse stability problem*, which, in turn, is a particular case of the general *inverse problem*:

> An inverse problem in science is the process of calculating from a set of observations the causal factors that produced them: for example, calculating an image in x-ray computed tomography, source reconstruction in acoustics, or calculating the density of the Earth from measurements of its gravity field. It is called an inverse problem because it starts with the effects and then calculates the causes. [9].

Inverse problems have wide application in many areas of science and technology. Below we will see how the inversion of the Vaccaro diagram can be effectively done and then discuss effects of the chromaticity, $x/y$ coupling, octupole tilts, and machine impedances.

## II. ONE-DIMENSIONAL CASE

Let us deal first with 1D case, when the nonlinearity is fed predominantly either from the $y$ plane (orthogonal to the plane of the collective mode) or from the $x$ plane, same as the one of the collective mode. Let it also be assumed that the nonlinearity is of the lowest order, i.e., caused by octupoles, so that $\Delta\omega(J_x, J_y) = kJ_y$ for the *alien* case, or $\Delta\omega(J_x, J_y) = kJ_x$ for the *own* case. Without compromising any generality, we may assume the octupole strength $k > 0$ and choose such units of the actions that $k = 1$. In this situation, the dispersion equation reduces to

$$\left[\int \mathrm{d}J_y \frac{F_y(J_y)}{\nu - J_y + io}\right]^{-1} = g \quad (7)$$

for the alien case. For the own one, it is obtained from here by the substitutions $J_y \to J_x$ and $F_y \to -J_x \frac{\partial F_x}{\partial J_x}$. Examples of 1D own and alien Vaccaro diagrams for the normalized Gaussian distribution $F(J_x, J_y) = \exp(-J_x - J_y)$ are presented in Fig. 1. Note that both diagrams are essentially

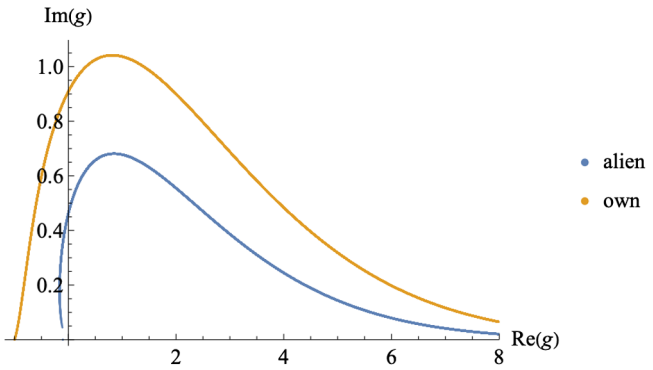


FIG. 1. Normalized Vaccaro diagrams for the Gaussian distribution when the octupole nonlinearity is fed from the alien (blue) or own (yellow) planes. The emittances and nonlinearity coefficients are unitary. Both curves scale linearly in both directions with the emittances and nonlinearity coefficients.

single-sided, mostly located at $\Re g > 0$. For the negative nonlinearity, $k < 0$, the diagrams would be mirror-reflected, being nonzero essentially at the negative side of the abscissa. This single-sidedness of the diagram can be interpreted as a demonstration of a relatively small shift of the coherent tune by the octupole tune spread. In such a case, the resonance between the coherent and incoherent oscillations may occur only when the wake shifts the collective tune to the same direction where the incoherent tunes are shifted by the octupoles.

Below in this section we suggest two methods of getting 1D distribution function from the stability diagram.

### A. Core-fit

A straightforward possibility to proceed opens at sufficiently large $\nu$, so that $\int_\nu^\infty \mathrm{d}J_y F_y \ll 1$. In this case the dispersion integral of the last equation can be taken asymptotically:

$$\int \mathrm{d}J_y \frac{F_y(J_y)}{\nu - J_y + io} \simeq \frac{1}{\nu} - \pi i F_y(\nu). \tag{8}$$

Consequently, Eq. (7) reduces to a fairly simple form,

$$\nu + \pi i \nu^2 F_y(\nu) \simeq g, \tag{9}$$

or, for the real and imaginary parts of the gain,

$$\Re g \simeq \nu; \qquad \Im g \simeq \pi \nu^2 F_y(\nu). \tag{10}$$

Since the Vaccaro diagram is nothing but a function $\Im g(\Re g)$, the solution of the inversion problem for the tail particles follows,

$$F_y(\nu) \simeq \frac{\Im g(\nu)}{\pi \nu^2}. \tag{11}$$

As noted above, for the own case, the results are obtained by a substitution $F_y \to -J_x \frac{\partial F_x}{\partial J_x}$,

$$-\nu \frac{\partial F_x(\nu)}{\partial \nu} \simeq \frac{\Im g(\nu)}{\pi \nu^2}. \tag{12}$$

These asymptotic relations provide solutions for the tail or halo particles.

A possible way to solve the problem for the bunch core is to assume that the distribution function belongs to a certain family of functions with few free parameters, fitting them to the measured diagram within its core region. For example, one may try to do the fitting with a binomial distribution function $F(J) \propto (1 - J/J_0)^n$, with a scale parameter $J_0 > 0$, a power parameter $n \geq 0$, assuming $0 \leq J \leq J_0$. A special advantage of this choice is that the dispersion integrals can be analytically taken, being expressed in terms of the hypergeometric function both for the alien and own cases. If the core of the beam distribution can be well described by a smooth monotonic function, one may expect that such a choice for the fitting candidates would provide a sufficient accuracy for the diagram core. Note that $J_0 < 0$ and $n < -1$ for all $J \geq 0$ can be tried for such binomial distributions as well, with the same advantage of the analytical expression of the dispersion integral.

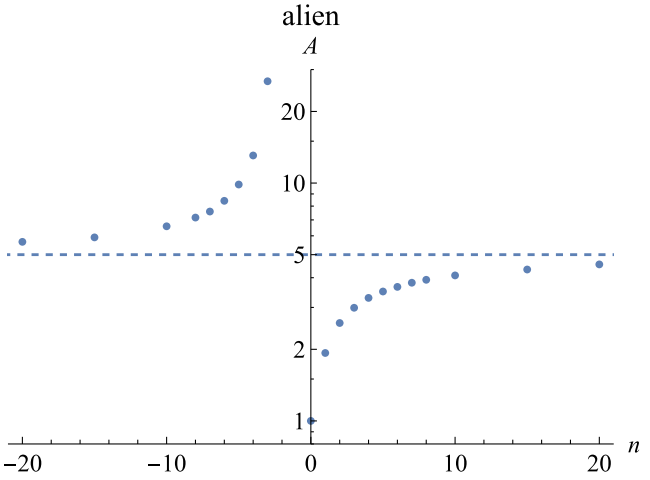


FIG. 2. Aspect ratio $A$ of 1D stability diagram, the alien case, versus the power $n$ of the binomial distribution function $\propto (1 - J/J_0)^n$, $nJ_0 > 0$. Note that $\lim_{n\to -2} A = \infty$. The dashed line marks the asymptote, $F(J) = J_0^{-1} e^{-J/J_0}$, $J_0 > 0$.

To facilitate work with this family of the fitting candidates, Figs. 2 and 3 provide plots for the aspect ratio of the stability diagram versus the power parameter $n$, for both alien and own cases. The aspect ratio $A$ is defined as a ratio of the diagram's full width at half maximum $\Delta \Re g_{\mathrm{FWHM}}$, to the maximum itself,

$$A = \Delta \Re g_{\mathrm{FWHM}} / \max \Im g. \tag{13}$$

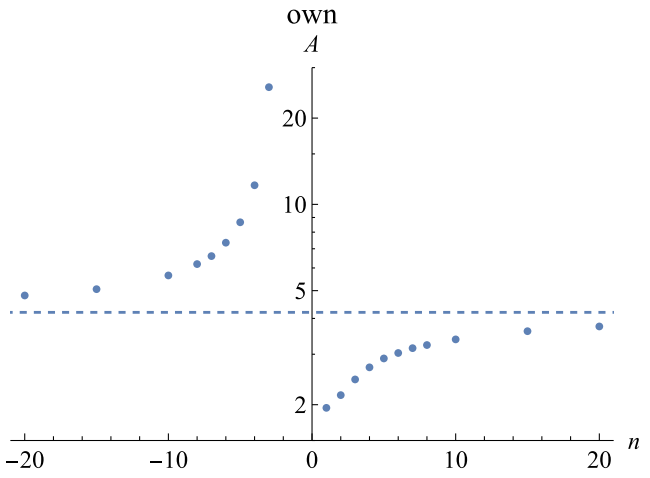


FIG. 3. The same as Fig. 2 for the own case. Here $\lim_{n\to -2} A = \infty$ as well.

One may use these plots in the following way: First, the aspect ratio $A$ of the measured diagram has to be computed. Then, the corresponding power parameter $n$ can be found from either Fig. 2 or Fig. 3, depending on the case. After that, the scaling parameter $J_0$ of the obtained binomial distribution can be found as a best fit to the measured diagram core. If the resulting agreement were not good enough, two options could be considered. The first one is to try a different family of the candidate functions, possibly with more fitting parameters. The second option is to use an iterative method with some initial guess function instead. An example of such a method is presented below.

### B. Iterative four-leg walk

Whatever the measured diagram is, we may consider the described binomial fit as an initial guess $F_{\text{in}}(J)$ for the sought-for distribution function. After that, we may do the following four consecutive steps: (1) Compute the dispersion integral of Eq. (7) numerically for sufficiently extended and dense set of the eigenvalues $\nu$ with the input distribution function $F_{\text{in}}(J)$, and so find $\Re g(\nu)$ as a table with possible interpolation. (2) Obtain the imaginary part $\Im g(\nu)$ for each value of the real part $\Re g(\nu)$ from the measured diagram. (3) Having thus the full complex gain $g(\nu) = \Re g(\nu) + i\Im g(\nu)$, compute an updated distribution function, $F_{\text{out}}(\nu) = -\pi^{-1}\Im g^{-1}(\nu)$. (4) Normalize the updated distribution, $F_{\text{out}}(\nu) \to F_{\text{out}}(\nu)/\int F_{\text{out}}(J)\mathrm{d}J$, and then use it as a new input at the first iterative step, $F_{\text{out}}(J) \to F_{\text{in}}(J)$. These four consecutive steps constitute an iterative *four-leg walk*, which can continue as long as needed.

The walk has to deal with some obstacles, however. The first one is clear for the alien case. As one can see in Fig. 1, a part of the alien diagram at the negative arguments is a two-valued function and each of its branches includes a point with infinite derivative, so the second leg stumbles at $\Re g \le 0$. To avoid this stumbling block, the involved interval of the actions $J$ (and thus, the eigenvalues $\nu$) can be limited from below, $\nu \ge \nu_{\text{min}}$, to guarantee that only positive values of the diagram abscissa are involved at step 2. However, the distribution at smaller actions, $J < \nu_{\text{min}}$, is needed at steps 1 and 4, so the extrapolation of the output distribution for those small arguments is needed. The second obstacle relates to the numerical stability and convergence of the process, which may require even larger lower border of the actions than the first obstacle requires.

Figure 4 demonstrates how the algorithm works for the Gaussian distribution, with $\nu_{\text{min}} = 0.7$. The convergence is extremely fast, but the algorithm gets numerically unstable at small actions, $J \lesssim 0.5$, for a lower value of the border $\nu_{\text{min}}$. The cost of the extrapolation is a possible loss of the distribution details at the area of small arguments, $J < \nu_{\text{min}}$.

The same algorithm can be applied to the own case too, of course. Since the stability diagram is everywhere a single-valued function now, as can be seen in Fig. 1, we might expect that the small-action problem will not appear. Such an expectation would be wrong, however. The instability problem at small actions takes place here as well, when the border $\nu_{\text{min}}$ is not sufficiently large. In fact, the stability may require even higher border here than for the alien case for the same actual and guess distributions. As a consequence, a deviation of the converged distribution from the actual one may be significant. This deviation can be reduced, however, since the stability requirement on $\nu_{\text{min}}$ is relaxed when the computed distribution moves closer to the actual one. An example of such iterations is presented in Fig. 5, where $\nu_{\text{min}}$ was reduced by almost a factor of 2 within the entire process. The corresponding behavior of the average emittance $\epsilon = \int JF\mathrm{d}J$ is shown in Fig. 6, where $\delta\epsilon$ is the difference between the computed and actual emittances.

Thus, we may conclude, that the suggested four-leg-walk algorithm seems to provide generally a fast convergence of

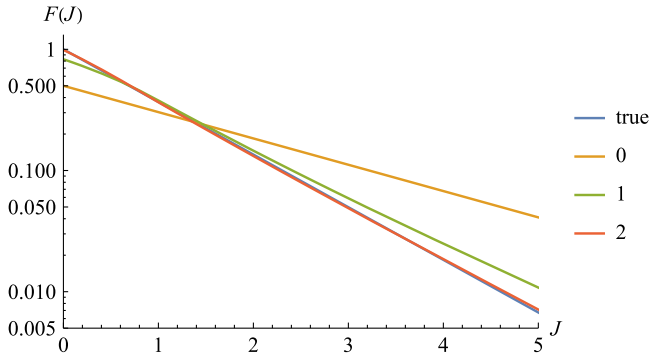


FIG. 4. An example of the iteration convergence for the alien case, $\nu_{\text{min}} = 0.7$. Here "true" means the distribution responsible for the "measured diagram"; "0" means the initial guess of the distribution, while "1" and "2" stand for the output distributions after the first and second four-leg moves of the algorithm. The latter is clearly very fast, but it becomes unstable at small actions, $J \lesssim 0.5$, for a slightly smaller border $\nu_{\text{min}}$.

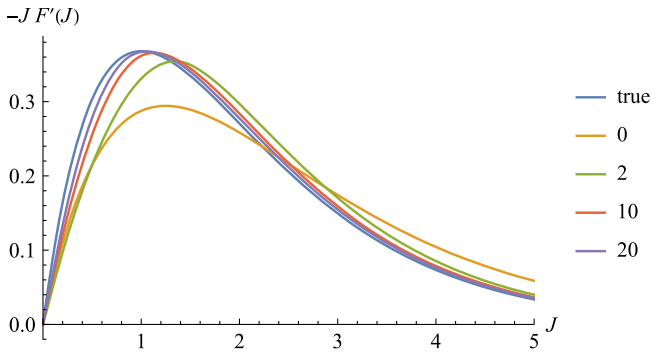


FIG. 5. Distribution convergence for the own case. The convergence parameter $\nu_{\text{min}}$ was reduced from 1.5 for the first four iterations to 1.2 for the next three iterations, then to 1.0 for the following two steps, and 0.8 till the end.

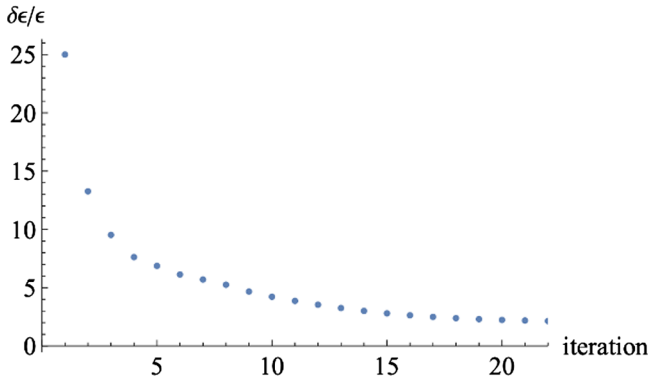


FIG. 6. Emittance convergence, in %, for the same case as in Fig. 5.

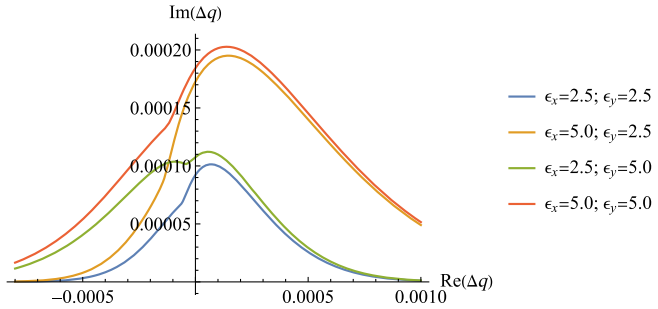


FIG. 7. Vaccaro diagrams calculated for a Gaussian bunch at the LHC top energy for 550 A of the octupole current, yielding $k_x = 1.0 \times 10^{-4}$, $k_y = 0.7 \times 10^{-4}$ for the normalized rms emittances 2.5 mm mrad; for more details see Ref. [5]. Gaussian normalized rms emittances for each curve are shown.

the computed distribution to the actual one. However, one should pay attention to the numerical stability and systematic deviation issues by following a proper strategy with the border parameter $\nu_{\min}$.

## III. TWO-DIMENSIONAL CASE

Let us move on now to a more general case, when the octupole nonlinearity is provided from both planes, $\Delta\omega(J_x, J_y) = k_x J_x - k_y J_y$. The reason why signs of the own and alien contributions are opposite here relates to the demonstrated single-sidedness of the 1D case, when the resonant particles effectively exist only for a certain sign of the real part of the coherent tune shift or the antidamper gain $\Re g$. For real beams, however, the coherent tune shifts may be of both signs, so their Landau damping requires the stability diagram to cover both positive and negative tune shifts. That is why the Landau octupoles have to provide, if possible, opposite signs of the own and alien contributions to the incoherent tune shifts. With this notation, assuming $k_{x,y} > 0$, suppression of collective modes with positive tune shifts requires sufficient $x$ emittance, while stability of the modes with negative tune shifts needs the same from the $y$ plane. This separation of $x/y$ responsibilities suggests an algorithm of the diagram inversion for the 2D case.

First, the halo distribution functions $F_y$ and $F_x$ can be found from Eq. (11), applied to the negative side of the diagram, and from Eq. (12), applied to the positive side, correspondingly. For the core distribution, the same fitting idea can be applied as for the 1D case, with the binomial or a similar distribution function within two sigmas or so. Again, the positive side of the diagram would be mostly affected by the $x$ emittance, and the negative side by the $y$ one.

Figure 7 illustrates how this $x/y$, or $+/-$ separation looks like in the example of the LHC octupoles and Gaussian bunches, as they were assumed in Ref. [5], at the top energy and for 550A of the octupole current. The coherent tune shift $\Delta q$ is taken there in the conventional units of the revolution frequency. The diagrams are computed for the normalized rms emittances, as they are specified there in the conventional mm mrad units. Note that doubling of the $x$ emittance approximately doubles the diagram scale at the positive side, making a much smaller effect at the negative side; the opposite is true for the $y$ emittance. That is why the 1D aspect ratios for the binomial distributions, Figs. 2 and 3, should provide good initial approximations for the 2D case too if the actual partial distributions are binomial or close to them. Keeping in mind the $+/-$ separation, one may see that the aspect ratios for the 2D Gaussian case of Fig. 7 are fairly close to the 1D numbers 5.0 (alien) and 4.2 (own).

Since both $F_y$ and $F_x$ distributions can be found from single-plane measurements, the method allows a consistency check by means of measuring the diagrams for both planes.

A question may be asked if it is possible to extend the 1D iterative four-leg-walk algorithm to 2D situation, or to invent for 2D another iterative algorithm. So far, I do not know the answer.

## IV. CHROMATICITY

The above consideration tacitly assumed that the chromaticity is negligible. If it is not, it can be taken into account as described below according to Ref. [10].

In a presence of the chromaticity, the antidamper excites all the headtail modes, whose coherent tune shifts $\Omega$ can be found from the following equation:

$$g \sum_{l=-\infty}^{\infty} \frac{K_l}{\Omega - l\omega_s} = 1, \tag{14}$$

with $g$ as the antidamper gain, $\omega_s$ as the synchrotron frequency. The form factors $K_l$ are determined by the rms headtail phase $\zeta$, which is the rms chromatic tune spread in the units of the synchrotron frequency,

$$K_l = \int_0^{\infty} \mathrm{J}_l^2(\zeta r) f(r) r \mathrm{d}r, \tag{15}$$

where $J_l$ is the Bessel function, and $f(r)$ is the normalized longitudinal phase space density,

$$\int_0^\infty f(r) r \mathrm{d}r = 1 \tag{16}$$

versus the radial amplitude $r$, whose units are chosen so that

$$\int_0^\infty f(r) r^3 \mathrm{d}r/2 = 1. \tag{17}$$

Note that

$$\sum_{l=-\infty}^{\infty} K_l = 1 \tag{18}$$

for any chromatic factor $\zeta$ and any distribution function $f(r)$. For the Gaussian bunch, $f(r) = \exp(-r^2/2)$, the form factor integrals can be analytically taken,

$$K_l(\zeta) = \exp(-\zeta^2) \mathrm{I}_l(\zeta^2), \tag{19}$$

where $I_l$ is the modified Bessel function. Plots of the first three form factors, together with their common asymptote, are presented in Fig. 8.

Let us reduce our analysis of Eq. (14) by the case of small or moderate chromaticity, $|\zeta| \lesssim 1$, considering two limit cases, a very small gain, $|g| \ll \omega_s$ and a very large one, $|g| \gg \omega_s$. In the former case, the gain is distributed among the headtail modes according to the form factors, so the coherent tune shifts for the headtail modes are

$$\Omega_l = l\omega_s + gK_l(\zeta). \tag{20}$$

In the latter case, the rigid-bunch mode is formed; it takes the entire gain, $\Omega = g$, so the chromaticity does not play a role. Due to its insensitivity to the chromaticity, this case presents a special interest for the suggested diagnostics.

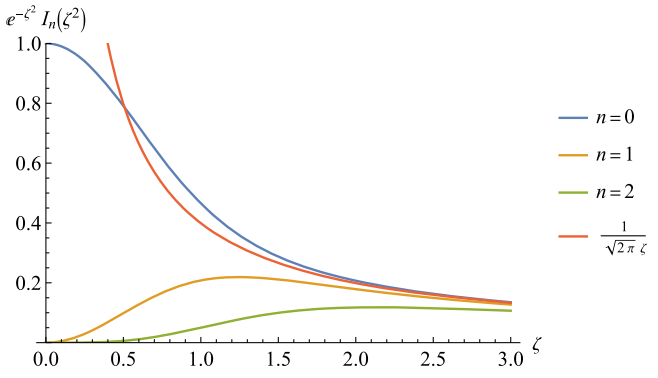


FIG. 8. Headtail form factors $K_n$ for a Gaussian bunch, together with their asymptote, versus the rms headtail phase $\zeta$.

Another benefit of a sufficiently large gain relates to the lesser effects of the machine impedances, whose knowledge is rather imprecise usually. Note that in case of larger chromaticity, $|\zeta| \geq 1$, this rigid-bunch regime requires $|g| \gg \omega_s|\zeta|$.

## V. OTHER FACTORS

Above, the machine optics was assumed to be uncoupled. In principle, the described diagnostics could work for coupled $x/y$ optics too. However, coupling would bring additional problems. For the coupled case, it is harder to control both the nonlinear optical coefficients $k$ of the Landau octupoles, and the coherent tune shifts of the antidamper. Also, for strong coupling, the octupole coefficients $k$ could drop dramatically, down to zero for circular modes.

A similar problem is associated with erratic tilts of the octupoles. If an octupole is tilted by an angle $\theta$, its effect decreases as $\cos(4\theta) \approx 1–8\theta^2$. Thus, the error bar of 1% or less requires $|\theta| \leq 2°$.

One more potential source of the error bars relates to the machine impedances, or the wakefields, as well as to the coherent effects of the image charges and currents. Indeed, such factors introduce their own, typically poorly known, coherent tune shifts and modify the beam response to the antidamper. To suppress such effects, high octupole and high gain settings would help. To make sure that those settings are high enough, the linear scaling of the diagram with the octupole strength could be checked.

For proton beams at low and medium energy, the space charge is almost always important. We did not consider it here, leaving this issue for future research. Another interesting area of the inverse stability problem, completely untouched here, is one associated with the alien longitudinal-to-transverse Landau damping.

## VI. SUMMARY

A novel method is suggested for finding beam phase space densities by means of the stability diagrams measured with an antidamper, with a further solution of an inverse stability problem.

Two algorithms are suggested for that matter, fitting and iterative ones. Their effectiveness and possible problems are demonstrated for the 1D case. For 2D diagram, the fitting algorithm should generally be as useful as for 1D cases. Generally, a single 2D diagram should allow to find two 1D phase space densities. The iterative algorithm is yet to be invented for 2D case.

Effects of the chromaticity, coupling, octupole tilts, and machine impedances are discussed.

Provided that the provoked instabilities are detected at their initial stage, and a sufficiently fast reduction of the gain follows, the suggested method can be nondestructive.

## ACKNOWLEDGMENTS

This manuscript has been authored by Fermi Research Alliance, LLC under Contract No. DE-AC02-07CH11359 with the U.S. Department of Energy, Office of Science, Office of High Energy Physics.

[1] H. Hereward, Landau damping by non-linearity, CERN, Geneva, Technical Report No. CERN-MPS-DL-69-11, 1969.

[2] A. Ruggiero and V. Vaccaro, Solution of the dispersion relation for longitudinal stability of an intense coasting beam in a circular accelerator (application to the ISR), CERN, Geneva, Technical Report No. CERN-ISR-TH/68-33, 1968.

[3] I appreciate historical investigations made by Elias Metral in this respect (2018).

[4] J. Scott Berg and F. Ruggiero, in *Proceedings of the Particle Accelerator Conference, Vancouver, BC, Canada, 1997* (IEEE, New York, 1997), Vol. 2, pp. 1712–1714.

[5] A. Burov, Phys. Rev. ST Accel. Beams **17**, 021007 (2014).

[6] E. Lifshitz and L. Pitaevskii, *Physical Kinetics* (Elsevier, New York, 1981), p. 268.

[7] A. W. Chao, *Physics of Collective Beam Instabilities in High Energy Accelerators* (Wiley, New York, 1993).

[8] S. A. Antipov, D. Amorim, N. Biancacci, X. Buffat, E. Métral, N. Mounet, A. Oeftiger, and D. Valuch, Phys. Rev. Lett. **126**, 164801 (2021).

[9] Wikipedia, Inverse Problem, July 9, 2022, https://en.wikipedia.org/wiki/Inverse_problem.

[10] A. Burov, Phys. Rev. Accel. Beams **21**, 114401 (2018).